High-frequency ultrasound combined with deep learning enables identification and size estimation of microplastics

Navid Zarrabi
Toronto Metropolitan University
Eric Strohm
Toronto Metropolitan University
Hadi Rezvani
Toronto Metropolitan University
Matthew Lisondra
University of Toronto
Nariman Yousefi
Toronto Metropolitan University
Sajad Saeedi
s.saeedi@ucl.ac.uk
University College London
Michael Kolios
Toronto Metropolitan University

Article

Keywords:

Posted Date: November 28th, 2025

DOI: https://doi.org/10.21203/rs.3.rs-8174921/v1

Additional Declarations: No competing interests reported.

Abstract

Microplastics are widespread in aquatic and terrestrial environments, yet standard identification techniques remain slow, labor-intensive, and unsuitable for large-scale or in-situ monitoring. In this work, we investigate high-frequency ultrasound as a fast, non-destructive alternative for microplastic detection, material identification, and size estimation. A peak-based extraction method isolated particle-specific echoes, from which temporal and spectral features were computed. We evaluated several machine learning methods and introduced a
one-dimensional convolutional neural network (1D-CNN) to classify material types. The proposed 1D-CNN achieved 99.75% accuracy, outperforming traditional models. Particle size was further estimated using material-specific multilayer perceptrons, which classified microspheres into four size ranges with up to 99.97% accuracy. These results show that
high-frequency ultrasound encodes discriminative scattering patterns that can be learned directly from raw acoustic signals, offering a fast and scalable framework for microplastic characterization with potential for future real-time or in-situ applications.

Introduction

Plastic pollution has become a global environmental crisis, prompting some to suggest a new geological epoch, the "Plasticene"[1]. As plastics degrade into microplastics (<5 mm) and nanoplastics (<1 μm)[2], their surface area and mobility increase, enabling them to act as vectors for persistent organic pollutants and heavy metals[3]. These particles have been detected in remote environments[4], as well as in soil[5], air[6], and even human tissues[7], including the brain, liver, and kidneys[8]. Their widespread distribution and bioaccumulation highlight the urgent need for effective detection and monitoring strategies[9].

Traditional microplastic (MP) identification techniques, such as Raman[10] and FTIR spectroscopy[11], pyrolysis-GC[12], and Scanning Electron Microscopy (SEM)[13], are
time-consuming, manual, and error-prone. While these methods are widely used, they are not well-suited for large-scale or in situ applications.

Ultrasound has shown promise as an alternative, but its use in microplastic detection remains underexplored[14]. Previous studies have demonstrated its potential: Falou et al.[15] and Baddour et al.[16] used high-frequency ultrasound to analyze microsphere backscatter, demonstrating agreement between theoretical and experimental results.
Meanwhile, Blevins et al.[17] demonstrated the feasibility of in-situ detection of polyethylene particles at lower frequencies.

Recent efforts have applied machine learning to improve traditional microplastic analysis workflows[18,19], but these approaches lack a fully automated classification of polymer types and particle size estimation. Deep learning-based studies have shown some success in polymer identification[20], though challenges

remain in validating mixed samples. Guselnikova et al.[21] proposed a pretreatment-free approach using a self-attention neural network, yet it only identifies polymer types and does not distinguish between materials or estimate particle size. Meanwhile, Han et al.[22] explored shape classification using photoacoustic imaging and generative models, but their method lacked material identification and required complex imaging not suited for in-situ use.

Ultrasound imaging offers an advantage by analyzing backscattered signals that carry information about material-specific properties such as density and acoustic impedance[17]. The choice of ultrasound frequency depends on the application: low frequencies (2–5 MHz) are used for deep tissue imaging[23], higher frequencies (>10 MHz) for high-resolution biomedical scans[24], and very low frequencies (<1 MHz) in industrial non-destructive testing[25,26]. Recent advances in machine learning have enhanced ultrasound signal interpretation[27,28], enabling applications like tissue characterization and fault detection.

Unlike previous work using 40 kHz ultrasound for large object detection[29], we utilize high-frequency ultrasound to classify MP material and size solely from backscattered signals. Higher frequencies enable more accurate identification of material types and particle sizes for MPs due to the smaller ultrasound wavelengths (on the order of micrometers). The application of high-frequency ultrasound for characterizing MPs represents a step forward in environmental sensing, offering a non-destructive, label-free method capable of determining particle properties at a microscale resolution. This work lays the foundation for real-time, in-situ monitoring of plastic pollution in complex aqueous environments. The proposed framework achieves an MP classification and size estimation accuracy of 99.75% and 99.97% for microspheres, respectively. The demonstrated ability to identify and size MPs using ultrasound alone may significantly reduce the dependence on a labor-intensive process. Such advancements could support policymakers and researchers in developing evidence-based strategies for managing plastic pollution.

Results

We designed a series of experiments using microspheres of various materials and sizes embedded in agarose phantoms to evaluate the proposed ultrasound-based framework for MP identification and size estimation. We developed a pipeline that systematically analyzes ultrasound backscatter data, which begins with signal acquisition and peak extraction, proceeds with material classification using machine learning and deep learning models, and concludes with particle size estimation (see the pipeline in Fig. 1).

Backscattered signals were acquired using a modified commercial acoustic microscope equipped with a 40 MHz transducer (see Methods). The transducers move across the sample in the x–y plane with a scanning step size of 10 μm, capturing ultrasound echo signals at each position (Fig. 1a, 1b). Maximum amplitude projections were generated for the visualization of these 3D tensors in 2D (Fig. 1c, 1d).

Simultaneously acquired optical microscopy images served as ground truth for validating the peak extraction method and assessing the accuracy of machine learning models (Fig. 1e). To collect training data, it was necessary to isolate acoustic signals reflected from microspheres from background noise. To achieve this, a peak extraction method was developed to identify signals with the highest absolute amplitude in the time domain, corresponding to the locations of microspheres and their reflections in maximum amplitude projection images. Peaks were detected using a sliding-window algorithm with an adaptive prominence threshold based on local image statistics (Fig. 1f, 1g). Manual validation against optical images confirmed a peak detection accuracy of 96.04% across a range of particle types and sizes, with the exception of overlapping or closely clustered particles. The detected peaks indicate the locations of the strongest reflected signals from individual particles. Following optical validation, these signals were incorporated into the dataset along with their corresponding material type and size labels.

Following the identification of signals reflected from microspheres, a labeled dataset was constructed with corresponding material types and particle sizes. These signals were analyzed in both the time and frequency domains to extract key acoustic features indicative of material composition[29] and particle size[16].

Each material exhibits distinct feature correlation patterns (Fig. 2). Across all material types, the most influential features were spectral spread, spectral entropy, and spectral centroid. An ablation study using the top-ranked features revealed that a subset of 13 features provided the highest classification accuracy. Spectral skewness and temporal crest factor were identified as the least impactful and were therefore excluded from the final feature set (Fig. 2e, 2f).

The variations in the correlation matrix (Fig. 2d) suggest that each material possesses unique descriptive features, reinforcing the rationale for using machine learning to identify such patterns. When the wavelength of the ultrasound is on the order of the particle's size, complex scattering patterns can be used to identify the particles. Particles have natural frequencies at which they vibrate strongly when excited, leading to unique spectral features associated with shape resonances. These resonance frequencies are related to the particle's size, shape, and material properties. One can identify the particles based on these resonances by analyzing the backscattered signal. Selected features (see Supplementary Table 1) collectively represent the signal’s statistical and spectral properties, facilitating the effective classification and analysis of different materials.

Table 1 summarizes the performance of various learning algorithms for material classification. Among the machine learning models, the multi-layer perceptron (MLP) achieved the highest accuracy, outperforming the Random Forest classifier and demonstrating the strength of neural networks for acoustic signal analysis. The proposed convolutional neural network model outperformed all other classifiers, achieving an accuracy of 99.75% with a standard deviation

Table 1

Classification Model Summary for Different Machine Learning Algorithms. CNN and MLP achieved the highest average performance across 10 experiments with varying random seeds. However, CNN outperformed all other models across all metrics, highlighting the advantage of automatic feature extraction tailored to material type over manually selected signal features applied uniformly to all materials.

Model	Accuracy (%)	Precision (%)	Recall (%)	F1-score (%)
K-Nearest Neighbors[30]	98.16 ± 0.24	97.84 ± 0.34	98.11 ± 0.21	97.96 ± 0.28
Logistic Regression[31]	87.56 ± 0.56	86.21 ± 0.64	84.93 ± 0.77	85.51 ± 0.70
Gradient Boosting[32]	98.01 ± 0.26	97.82 ± 0.33	97.97 ± 0.30	97.89 ± 0.31
Decision Tree[33]	97.37 ± 0.29	97.11 ± 0.32	97.24 ± 0.37	97.17 ± 0.31
SVM (RBF Kernel)[34]	97.23 ± 0.29	96.74 ± 0.32	97.20 ± 0.32	96.94 ± 0.32
PCA + Logistic Regression[35]	66.21 ± 0.44	49.96 ± 0.35	57.82 ± 0.43	53.18 ± 0.30
Voting Classifier[36]	98.15 ± 0.17	97.95 ± 0.22	98.16 ± 0.19	98.05 ± 0.20
Random Forest[37]	99.05 ± 0.25	98.85 ± 0.31	99.09 ± 0.25	98.97 ± 0.28
MLP[38]	99.52 ± 0.16	99.51 ± 0.17	99.53 ± 0.15	99.52 ± 0.15
1D CNN (proposed)	99.75 ± 0.18	99.73 ± 0.26	99.80 ± 0.14	99.76 ± 0.20

of 0.18% across 10 randomly selected train-test splits.

Figure 3 illustrates the maximum projection image of samples containing different types of microspheres. As shown in Fig. 3a-c, the network successfully detects and identifies all microspheres in samples containing only one type of microsphere with the same size, even those in close proximity to each other. To further evaluate the method, the model has been tested on mixed samples, as depicted in Fig. 3d-g. Particles that are not spatially overlapping or in close proximity are accurately detected and identified, as shown in Fig. 2d. The network also demonstrates the ability to identify particles of the same size and type that are positioned closely together, as seen in Fig. 3e.

For size estimation, we leveraged the fact that backscatter spectral profiles scale predictably with particle diameter[16]. To capture these patterns, material-specific multilayer perceptrons (MLPs) were trained using labeled signals. Sizes were grouped into four categorical bins (20–28 μm, 38–57 μm, 67–90 μm, 300–330 μm), and predicted using softmax output layers. This approach achieved 100% classification accuracy for PE, PMMA, and steel, and 99.97% for glass microspheres.

Discussion

Machine learning algorithms achieved results comparable to those of the CNN, largely due to the comprehensive set of features extracted from both the time and frequency domains. However, the CNN consistently outperformed them across all performance metrics. This superior performance is attributed to the CNN's ability to learn and extract relevant features directly from the data automatically. Unlike traditional machine learning models that rely on manually engineered features, convolutional neural networks (CNNs) automatically learn and extract the most discriminative patterns necessary for accurate classification.

Challenges arise when a high density of small steel microspheres is present in a confined region. In such cases, the peak extraction algorithm fails to detect all peaks, and for those detected, the network struggles with accurate classification (Fig. 3f). Additionally, when two particles of different types are in close proximity, one may be overlooked if the other has significantly stronger backscattering. For instance, when PE and glass microspheres are close together, the peak extraction algorithm does not detect the glass particle due to the stronger backscatter signals of PE (Fig. 3f).

Similarly, when two particles of the same type but different sizes are near each other, the peak extraction algorithm often fails to detect both. If one signal is significantly stronger, the peak extraction algorithm tends to identify only the particle with the dominant signal (Fig. 3g). More broadly, scattering patterns resulting from shape resonance frequencies can be clearly resolved in suspension. In practice, heterogeneity in particle shape, surface roughness, matrix effects (e.g., high salinity), and aggregation may blur these acoustic signatures. Non-spherical shapes and overlapping particles may lead to ambiguous or non-unique scattering responses. It is expected that the methods developed based on deep learning will be more robust to such heterogeneities than model-based inversion approaches that use a theoretical forward model

(e.g., Faran scattering theory) and iteratively adjust parameters to minimize the error between the model and experimental data, thereby estimating microplastic size and material composition.

This approach using CNNs will provide the foundation for future investigations designed to test the technique's resilience to the heterogeneities mentioned above. Despite potential limitations, the application of high-frequency ultrasound holds significant promise for identifying microplastics (MPs), addressing a critical need in environmental science. Due to their small size and diverse composition, MPs pose a significant challenge to existing detection and characterization methods. Inspired by the demonstrated relationship between particle size, composition, and acoustic scattering properties in this study, high-frequency ultrasound can offer a novel approach.

Specifically, by analyzing the scattering patterns of microparticles in suspension, it may be possible to determine both the size and material composition of individual MP particles. The method can differentiate between plastic materials, provided there is a sufficient difference in their density and speed of sound. This technique could enable more accurate quantification of MP pollution in various environmental matrices, leading to more informed assessments of their ecological impact and the development of more effective mitigation strategies. Future strategies may incorporate the use of

acoustic flow cytometry, whereby the scattering of thousands of particles are analyzed in a custom US system to rapidly acquire the signals from particles flowing in a microfluidic device[39].

Figure 3| Material type prediction of samples containing single and mixed microspheres. a-c, The network accurately identifies microsphere types in single-material samples, even in cases of overlapping particles. As each sample contains only one particle type, ground-truth optical images were not required for validation.

d, Representative acoustic and optical images of mixed-material samples, showing successful identification of all particles. **e**, The network correctly predicts particle types even when particles of the same size and type are closely spaced. **f**, Performance degrades in densely packed regions, where overlapping particles reduce detection accuracy; **g**, In some cases, smaller particles adjacent to larger ones are missed due to the dominant backscatter signal of the larger particle.

Methods

Ultrasound Imaging System

Backscattered signals, generated when ultrasound waves interact with materials of varying acoustic properties, provide insights into a sample's structure and composition. This study utilized a modified commercial acoustic microscope (Kibero GmbH, Saarbrücken, Germany) equipped with simultaneous optical imaging to acquire both backscattered signals and optical images, following the signal acquisition mechanism described by Strohm et al.[39]. Additional specifications of the modified acoustic microscope are provided in the Supplementary Appendix.

Sample Preparation

To evaluate the proposed detection and classification framework, microspheres of plastic (PMMA, PE) and non-plastic (steel, glass) materials were used. Polyethylene (PE), steel, and glass microspheres were purchased from Cospheric LLC (Santa Barbara, CA, USA). PMMA microspheres were obtained from Lab261 (Palo Alto, CA, USA). The microspheres were acquired in four nominal size ranges: 20–28 μm, 38–57 μm, 67–78.5 μm, and 300–330 μm. Particles were embedded in a 2% agarose gel phantom. To ensure uniform distribution, plastic microspheres were mixed directly into the gel. For denser particles, such as glass and steel, a two-layer design was employed to prevent settling, thereby allowing all particles to remain in the acoustic focal plane (Fig. 1a).

Frequency Requirements

The selection of ultrasound frequency is critical, as it directly determines the minimum particle size that can be reliably detected. Higher frequencies are required to detect smaller particles due to their shorter wavelengths and enhanced sensitivity to fine-scale structures.

Using ultrasound with wavelengths approximately the same size as the object offers a unique advantage for identifying material composition and structural characteristics due to enhanced**Fig. 4| Scattering spectra of microspheres composed of different materials, computed over the 0–100 MHz range using Faran's theory.** The model predicts the first resonance peak for PMMA microspheres at 37.5 MHz, establishing this frequency as the minimum threshold for reliable detection. Spectral analysis indicates that lower frequencies produce insufficient scattering, limiting their effectiveness for detecting 20 μm particles.

sensitivity to wave-object interactions.

To explore the appropriate range of ultrasound frequencies for easier discrimination between the size and composition of MPs, the extended version of Faran's theory by Hickling[40,41] is utilized. This theory describes the scattering of acoustic waves upon encountering a spherical object, where the scattered wave is influenced by the object's size, the properties of the surrounding medium, and the observation angle. The governing equation accounts for the interaction of different frequency components with the sphere, resulting in phase shifts and intensity variations. According to Faran's theory, the scattered pressure field P_s is given by:

$$P_s(\theta, f) = \frac{P_0}{akr} \sum_{n=0}^{\infty} \left[(-i)^n (2n+1) \sin\eta_n \ \exp(-i\eta_n) P_n(\cos\theta)\right] \times \exp(-ikr)$$

1

where P_0 denotes the initial ultrasound pressure, and r is the distance to the observation point. The P_n is the Legendre polynomial of order n. The wave number is defined as $k = \frac{2\pi f}{c}$, where f is the frequency and c is the speed of sound. The parameter a is the radius of the scattering object, and η_n is a phase angle. This angle depends on the dimensionless quantity $\mathrm{k_a}$, the properties of the coupling fluid, and the Poisson's ratio of the cell. The equation models both shear and compressional wave components in the sample.

Faran's scattering theory was used to evaluate the frequency-dependent backscattered response over the range of 0–100 MHz (Fig. 4). This spectral analysis revealed that 20 μm PMMA microspheres produce their first detectable shape resonance at approximately 37 MHz, establishing 40 MHz as a practical lower bound for detecting all particle types in this study. Below this frequency, the scattering strength decreases by approximately 50 dB, resulting in a significantly reduced signal-to-noise ratio (SNR) and making reliable detection increasingly difficult. In contrast, other microsphere types exhibit their primary resonances at lower frequencies. Accordingly, a center frequency of 40 MHz is sufficient to enable the detection of all microsphere types examined in this study. This choice is further supported by finite-element simulations of microsphere scattering behavior, which confirm shape resonances and surface modes in this frequency range[42]. As every other microsphere used in this study exhibited

resonance at even lower frequencies, a 40 MHz transducer was selected to ensure consistent detection across all microspheres.

Peak Extraction

The backscattered signals, captured in the time domain by transducers using the time-of-flight approach, provide crucial information about the medium they traverse. By analyzing the signals and their Fourier transform, salient features such as energy, peak amplitude, and signal attenuation can be extracted, offering insights into the material's characteristics[29] and size[16].

Backscattered signals stem from microspheres of varying material types and sizes. Stronger signals, characterized by higher SNR, provide more reliable and accurate information about the backscattered material. Several methods exist for peak extraction. A commonly used approach is threshold-based detection[43], which is computationally efficient but highly sensitive to noise and relies on manually selected thresholds. Another approach is derivative-based peak extraction[44], which identifies peaks by detecting changes in slope. However, this method often detects all global and local peaks without considering their prominence, making it prone to misclassifying noise as peaks. Machine learning methods have also been applied for peak extraction[45]. These techniques can be highly effective but require a sufficient amount of labeled data to train the network, ensuring it can generalize to unseen peak structures. In this study, a sliding-window-based approach is proposed, augmented with signal smoothing based on the data's standard deviation. This method effectively isolates the signals with the highest maximum amplitude from the 3D array while minimizing the impact of noise and irrelevant peaks.

To extract the peaks from the amplitude image, first, the maximum amplitude is identified as shown in the 3D visualization (Fig. 1f). Then, a sliding window approach was applied to identify prominent maxima based on a prominence threshold defined as $(\mu + \alpha \rho_s)$, where α is an adjustable parameter for each acoustic image and ρ_s represents the standard deviation within the sliding window region. The peak extraction process is detailed in Supplementary Algorithm 1.

Features Extraction

The reference dataset consists of signals in the time domain along with their material and size labels. The frequency-domain representations of these signals are then computed using the Fast Fourier Transform (FFT)[46]. By extracting features that characterize both the temporal and spectral domains, it becomes feasible to infer the composition of the scattering medium[47]. In this study, a total of 15 features were extracted, with 4 derived from the temporal signals and 11 from the spectral signals, as summarized in Supplementary Table 1. These features were subsequently used as inputs to machine learning models for predicting the material type of the microspheres.

Material Identification using Machine Learning

To identify the type of material using its echo signal, various machine learning methods can be applied. For this purpose, the backscattered signals from different materials have been used as labeled training data. For this purpose, the backscattered signals from different materials were used as labeled training data (see Supplementary Appendix for labeling details). Different classification algorithms were applied to the labeled data, as shown in Table 1. All algorithms were executed with 10 different random seeds, and their mean and standard deviation were reported. The MLP had two layers of 80 neurons, and the Voting Classifier was set with soft voting on ensembles of Linear Regression, Random Forest, and Gradient Boosting to get their best performance. The results show that these features can be descriptive of the type of material and also the capability of learning methods in material classification. Among machine learning algorithms, MLP and Random Forest outperformed the others using all extracted features.

To further improve classification performance and eliminate the need for handcrafted features, we implemented a one-dimensional convolutional neural network (1D CNN) trained directly on the Fourier Transform of the backscattered signals. The network architecture, described in detail in the Supplementary Appendix, was designed to extract temporal patterns from each signal using multiple convolutional layers with varying kernel sizes and pooling strategies. Global max pooling and dropout layers were used to retain critical features and minimize overfitting. The final dense layers performed softmax-based classification across four material types.

Training and Evaluation

All models were trained using the signals extracted from microspheres in the acoustic images. Reflections from individual microspheres were identified using the proposed peak detection and labeling method. To capture the signals reflected from each microsphere, a 5 × 5 spatial array of signals was constructed, centered on the point of the strongest absolute global maximum in the maximum projection image. In total, 25 signals per particle were extracted and stored in the dataset from each maximum projection image. A total of 8,045 signals were extracted and categorized into four classes: PMMA (1,525 signals), steel (2,210 signals), PE (1,195 signals), and glass (3,115 signals). For classification, peak extraction was performed to isolate the backscattered signals from each microsphere, which was then fed into the trained model for prediction. To assess the model's generalization ability and prevent overfitting, test images containing particles not seen during training were used in the evaluation phase.

Size Estimation

The backscatter response for spheres with identical mechanical properties but varying sizes follows the same curve, with differences appearing as a stretch along the frequency axis proportional to the sphere's diameter[16]. To utilize this characteristic, material-specific MLPs have been trained for each material type. The MLP architecture consists of an input layer, two hidden layers with ReLU activation, and an

output layer. Given the manufacturer-specified size ranges of the microspheres, they have been categorized into bins: 20–28μm, 38–57μm, 67–90μm, and 300–330μm. By framing the size estimation as a classification problem, the output layer with softmax activation predicts probabilities for each size class, enabling precise categorical classification.

Declarations

Author contributions

N.Z. conceived the study, developed the analysis pipeline, performed formal analysis, and wrote the original draft. E.S. designed the experimental ultrasound system and supervised data acquisition. H. R. contributed to the literature review and manuscript revision. M.L. developed the semi-automated annotation pipeline and wrote the corresponding section. N.Y. supervised the project, contributed to methodology development, and edited the manuscript.
S.S. supervised the project, contributed to methodology development, and edited the manuscript. M. K. provided resources, supervised the ultrasound imaging experiments, and offered critical feedback throughout the study.

Funding

This work was supported by the Environment and Climate Change Canada's (ECCC) Increasing Knowledge on Plastic Pollution Initiative (Grant No. GCXE21S057), the Social Sciences and Humanities Research Council of Canada's (SSHRC) New Frontiers in Research Fund - Exploration program (Grant No. NFRFE-2022-00746), and the Natural Sciences and Engineering Research Council of Canada's (NSERC) Discovery Grants program awarded to Nariman Yousefi (Grant No. RGPIN-2020-04659). Additional support was provided by the Natural Sciences and Engineering Research Council of Canada's (NSERC) Discovery Grants program awarded to Sajad Saeedi (Grant No. RGPIN-2020-05436).

Competing interests

All authors declare no financial or non-financial competing interests.

Data availability

Data and code have been deposited on Code Ocean. An anonymized version will be provided to reviewers during the peer-review process. A permanent DOI will be shared upon acceptance.

References

1. Rangel-Buitrago, N., Neal, W. & Williams, A. The Plasticene: time and rocks. *Mar. Pollut. Bull.* 185, 114358 (2022).
2. Lai, H., Liu, X. & Qu, M. Nanoplastics and Human Health: Hazard Identification and Biointerface. *Nanomater. Basel* 12, 1298 (2022).
3. Brennecke, D., Duarte, B., Paiva, F., Caçador, I. & Canning-Clode, J. Microplastics as vector for heavy metal contamination from the marine environment. *Estuar. Coast. Shelf Sci.* 178, 189–195 (2016).
4. Chen, Q. *et al.* Long-range atmospheric transport of microplastics across the southern hemisphere. *Nat. Commun.* 14, 7898 (2023).
5. Ai, W., Chen, G., Yue, X. & Wang, J. Application of hyperspectral and deep learning in farmland soil microplastic detection. *J. Hazard. Mater.* 445, 130568 (2023).
6. Gasperi, J. *et al.* Microplastics in air: are we breathing it in? *Curr. Opin. Environ. Sci. Health* 1, 1–5 (2018).
7. Wu, P. *et al.* Absorption, distribution, metabolism, excretion and toxicity of microplastics in the human body and health implications. *J. Hazard. Mater.* 437, 129361 (2022).
8. Nihart, A. J. *et al.* Bioaccumulation of microplastics in decedent human brains. *Nat. Med.* 1–6 (2025).
9. Yates, J. *et al.* Plastics matter in the food system. *Commun. Earth Environ.* 6, 176 (2025).
10. Ribeiro-Claro, P., Nolasco, M. M. & Araújo, C. Characterization of microplastics by Raman spectroscopy. *Compr. Anal. Chem.* 75, 119–151 (2017).
11. Hernandez, L. M., Yousefi, N. & Tufenkji, N. Are there nanoplastics in your personal care products? *Environ. Sci. Technol. Lett.* 4, 280–285 (2017).
12. Fries, E. *et al.* Identification of polymer types and additives in marine microplastic particles using pyrolysis-GC/MS and scanning electron microscopy. *Environ. Sci. Process. Impacts* 15, 1949–1956 (2013).
13. Wang, Z.-M., Wagner, J., Ghosal, S., Bedi, G. & Wall, S. SEM/EDS and optical microscopy analyses of microplastics in ocean trawl and fish guts. *Sci. Total Environ.* 603, 616–626 (2017).
14. Abimbola, I., McAfee, M., Creedon, L. & Gharbia, S. In-situ detection of microplastics in the aquatic environment: A systematic literature review. *Sci. Total Environ.* 173111 (2024).
15. Falou, O., Rui, M., El Kaffas, A., Kumaradas, J. C. & Kolios, M. C. The measurement of ultrasound scattering from individual micron-sized objects and its application in single cell scattering. *J. Acoust. Soc. Am.* 128, 894–902 (2010).
16. Baddour, R. E., Sherar, M. D., Hunt, J., Czarnota, G. & Kolios, M. C. High-frequency ultrasound scattering from microspheres and single cells. *J. Acoust. Soc. Am.* 117, 934–943 (2005).
17. Blevins, M. G. *et al.* Field-portable microplastic sensing in aqueous environments: a perspective on emerging techniques. *Sensors* 21, 3532 (2021).
18. Weber, F., Zinnen, A. & Kerpen, J. Development of a machine learning-based method for the analysis of microplastics in environmental samples using µ-Raman spectroscopy. *Microplastics*

Nanoplastics 3, 9 (2023).

19. Han, X.-L. *et al.* Deep learning based approach for automated characterization of large marine microplastic particles. *Mar. Environ. Res.* 183, 105829 (2023).
20. Rezvani, H. *et al.* Morphological Detection and Classification of Microplastics and Nanoplastics Emerged from Consumer Products by Deep Learning. *ArXiv Prepr. ArXiv240913688* (2024).
21. Guselnikova, O. *et al.* Pretreatment-free SERS sensing of microplastics using a self-attention-based neural network on hierarchically porous Ag foams. *Nat. Commun.* 15, 4351 (2024).
22. Han, K. *et al.* Innovative methods for microplastic characterization and detection: Deep learning supported by photoacoustic imaging and automated pre-processing data. *J. Environ. Manage.* 359, 120954 (2024).
23. Fu, J., Zhou, X., Chen, L. & Lu, S. Abdominal ultrasound and its diagnostic accuracy in diagnosing acute appendicitis: a meta-analysis. *Front. Surg.* 8, 707160 (2021).
24. Russo, A. *et al.* Clinical application of ultra-high-frequency ultrasound. *J. Pers. Med.* 12, 1733 (2022).
25. Gupta, M., Khan, M. A., Butola, R. & Singari, R. M. Advances in applications of Non-Destructive Testing (NDT): A review. *Adv. Mater. Process. Technol.* 8, 2286–2307 (2022).
26. Shi, X. Application of ultrasonic non-destructive testing in industrial pipeline inspection. *Appl. Math. Nonlinear Sci.* 9,.
27. Deeba, F. *et al.* A multiparametric volumetric quantitative ultrasound imaging technique for soft tissue characterization. *Med. Image Anal.* 74, 102245 (2021).
28. Rautela, M. & Gopalakrishnan, S. Ultrasonic guided wave based structural damage detection and localization using model assisted convolutional and recurrent neural networks. *Expert Syst. Appl.* 167, 114189 (2021).
29. Sahoo, A. K. & Udgata, S. K. Material Classification based on Non-contact Ultrasonic Echo Signal Using Deep Learning Approach. *Procedia Comput. Sci.* 235, 606–616 (2024).
30. Cover, T. M. & Hart, P. E. Nearest neighbor pattern classification. *IEEE Trans. Inf. Theory* 13, 21–27 (1967).
31. Cox, D. R. The regression analysis of binary sequences. *J. R. Stat. Soc. Ser. B Methodol.* 20, 215–232 (1958).
32. Friedman, J. H. Greedy function approximation: a gradient boosting machine. *Ann. Stat.* 1189–1232 (2001).
33. Breiman, L. *Classification and Regression Trees*. (Routledge, 2017).
34. Cortes, C. & Vapnik, V. Support-vector networks. *Mach. Learn.* 20, 273–297 (1995).
35. Jolliffe, I. T. *Principal Component Analysis*. vol. 2 (Springer, 2002).
36. Kuncheva, L. I. & Whitaker, C. J. 'That' elusive diversity in classifier ensembles. *Pattern Recognit.* 36, 241–264 (2003).
37. Breiman, L. Random forests. *Mach. Learn.* 45, 5–32 (2001).
38. LeCun, Y., Bengio, Y. & Hinton, G. Deep learning. *Nature* 521, 436–444 (2015).

39. Strohm, E. M., Czarnota, G. J. & Kolios, M. C. Quantitative measurements of apoptotic cell properties using acoustic microscopy. *IEEE Trans. Ultrason. Ferroelectr. Freq. Control* 57, 2293–2304 (2010).
40. Faran Jr, J. J. Sound scattering by solid cylinders and spheres. *J. Acoust. Soc. Am.* 23, 405–418 (1951).
41. Hickling, R. Analysis of Echoes from a Solid Elastic Sphere in Water. *J. Acoust. Soc. Am.* 34, 1582–1592 (1962).
42. Falou, O., Jafari Sojahrood, A., Carl Kumaradas, J. & Kolios, M. C. Surface modes and acoustic scattering of microspheres and ultrasound contrast agents. *J. Acoust. Soc. Am.* 132, 1820–1829 (2012).
43. Jacobson, A. L. Auto-threshold peak detection in physiological signals. in 2001 *Conference Proceedings of the 23rd Annual International Conference of the IEEE Engineering in Medicine and Biology Society* vol. 3 2194–2195 vol.3 (2001).
44. Luo, S. *et al.* Developing a peak extraction and retention (PEER) algorithm for improving the temporal resolution of Raman spectroscopy. *Anal. Chem.* 93, 8408–8413 (2021).
45. Sumukha, B. N., Kumar, R. C., Bharadwaj, S. S. & George, K. A novel approach to peak detection using sequential learning algorithm. in 2016 *2nd International Conference on Contemporary Computing and Informatics (IC3I)* 862–867 (2016). doi:10.1109/IC3I.2016.7918803.
46. Brigham, E. O. & Morrow, R. E. The fast Fourier transform. *IEEE Spectr.* 4, 63–70 (1967).
47. Krause, D., Hussein, W. B., Hussein, M. A. & Becker, T. Ultrasonic sensor for predicting sugar concentration using multivariate calibration. *Ultrasonics* 54, 1703–1712 (2014).

Figures

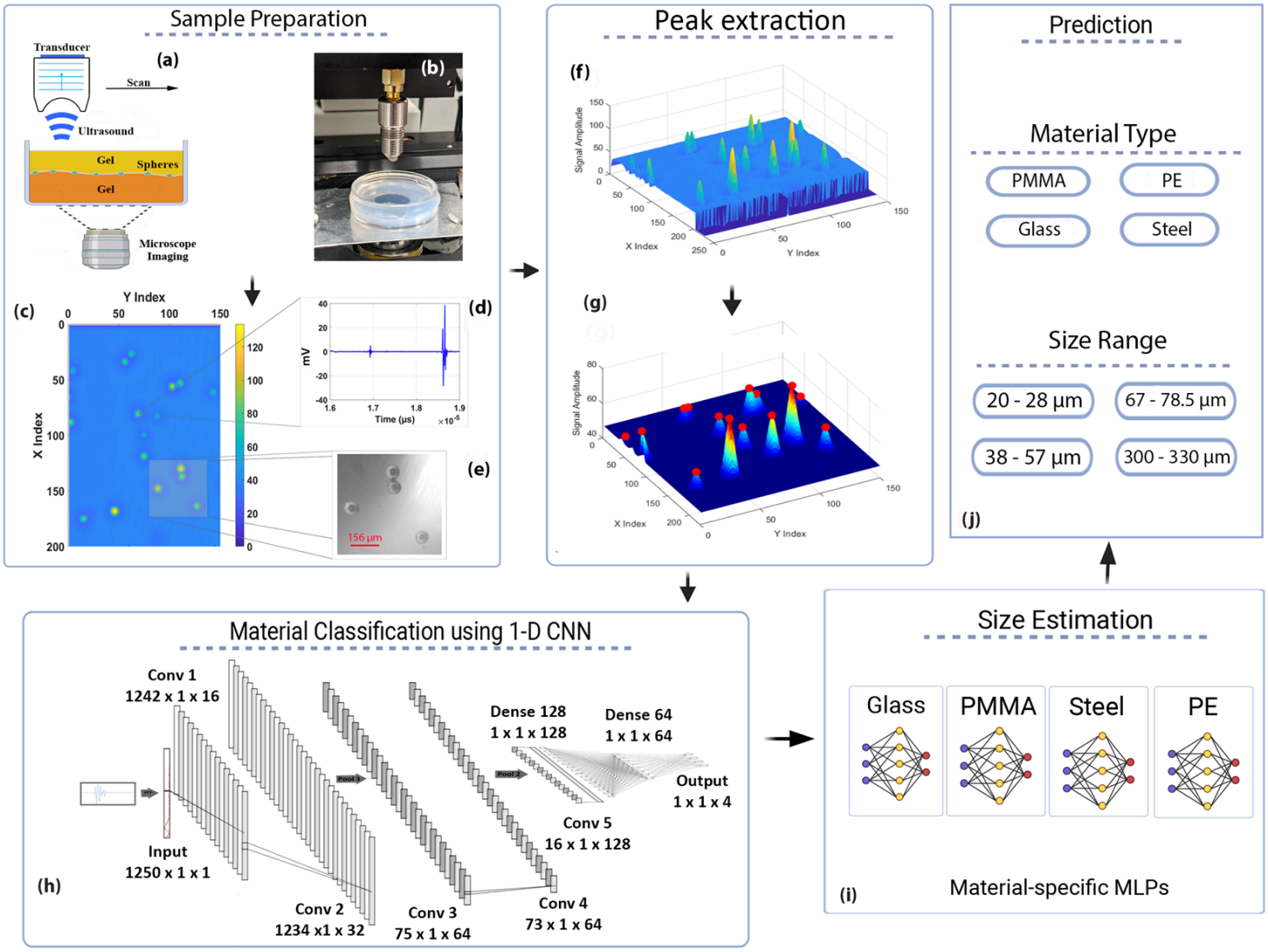

Figure 1

Overview of the MP analysis pipeline, including sample preparation, signal acquisition, peak extraction, material classification, and size estimation. a-b, Acoustic imaging was performed using a single-element transducer positioned above the sample, with scanning controlled by a motorized translation stage. **Optical images** were acquired using an IX71 microscope, enabling ground-truth validation of acoustic data. **c,** Backscattered ultrasound signals were recorded in the time domain, forming a 3D tensor where x and y represent spatial coordinates and the third dimension corresponds to time (time of flight). Maximum amplitude projections were used for the visualization of signals in 2D. **d,** Each pixel in the projection image represents the maximum amplitude of a backscattered signal, with the corresponding temporal signal stored for downstream analysis. **e,** Optical microscopy images were acquired from the same sample regions to serve as ground truth for validating peak extraction and machine learning predictions.

f-g,Peak extraction was performed using a sliding-window method with a data-adaptive prominence threshold ($\mu + \alpha\sigma$), where α is user-defined and σ is the local standard deviation. **h,** Fast Fourier Transform (FFT) is applied to the backscattered signals from particles extracted in the previous step.

The FFT transform of these signals is then used to train a 1D convolutional neural network (CNN) for material classification. The network architecture learns hierarchical temporal features through progressively smaller convolution kernels and max-pooling layers, enabling direct classification from raw acoustic waveforms. **i,** Size estimation was performed using material-specific MLPs, trained to classify microspheres into four discrete size bins (20–28 μm, 38–57 μm, 67–90 μm, and 300–330 μm) using softmax-based output probabilities.

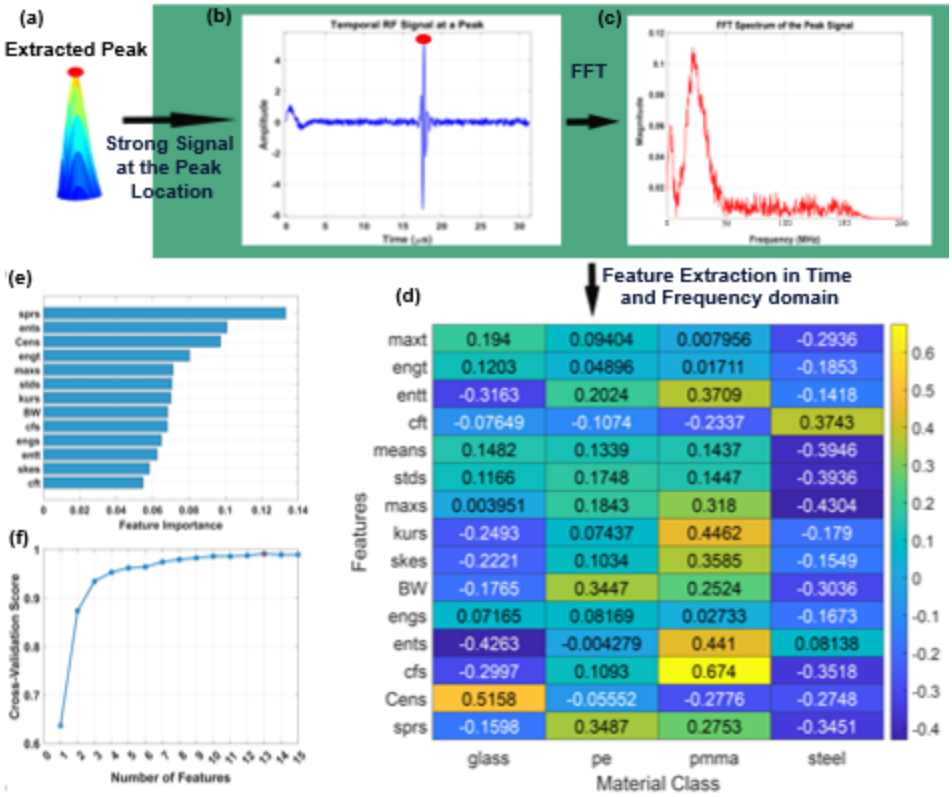

Figure 2

Feature extraction from the temporal and spectral domains of the strongest backscattered signals. a, The peak extraction algorithm identifies the locations of highest maximum-amplitude backscattered signals, indicating the presence of potential objects. **b**, Temporal signal amplitudes are analyzed at the identified peak locations. **c**, The FFT is applied to the temporal signals to obtain their spectral representations, from which spectral features are extracted. **d**, The correlation matrix between features and material types shows that each material exhibits distinct associations with specific features. For example, glass is most strongly correlated with spectral centroid (Cens) and spectral entropy (ents), while PMMA is correlated with spectral crest factor (cfs) and spectral kurtosis (kurs). **e**, Feature importance analysis based on correlations with material labels indicates that spectral spread (sprs) is the most important feature, whereas the temporal crest factor is the least important. **f**, A Random Forest model was trained using subsets of 1 to 15 features, ranked by importance, to determine the minimum number of features required. The results show that using 13 features yields the highest classification accuracy, indicating the optimal feature set for material type prediction.

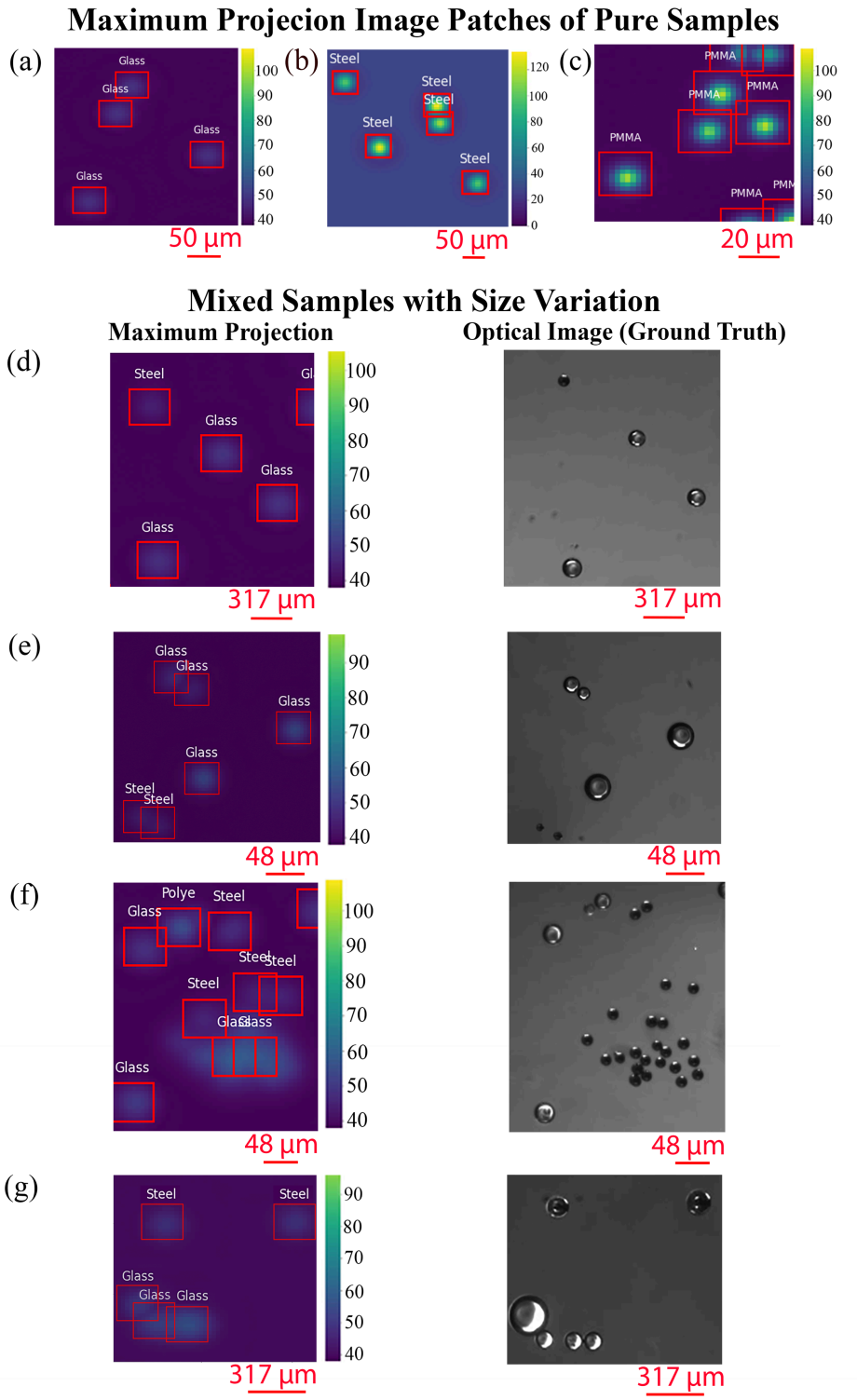

Figure 3

Material type prediction of samples containing single and mixed microspheres. a-c, The network accurately identifies microsphere types in single-material samples, even in cases of overlapping particles. As each sample contains only one particle type, ground-truth optical images were not required for validation.

d, Representative acoustic and optical images of mixed-material samples, showing successful

identification of all particles. **e,** The network correctly predicts particle types even when particles of the same size and type are closely spaced. **f,** Performance degrades in densely packed regions, where overlapping particles reduce detection accuracy; **g**, In some cases, smaller particles adjacent to larger ones are missed due to the dominant backscatter signal of the larger particle.

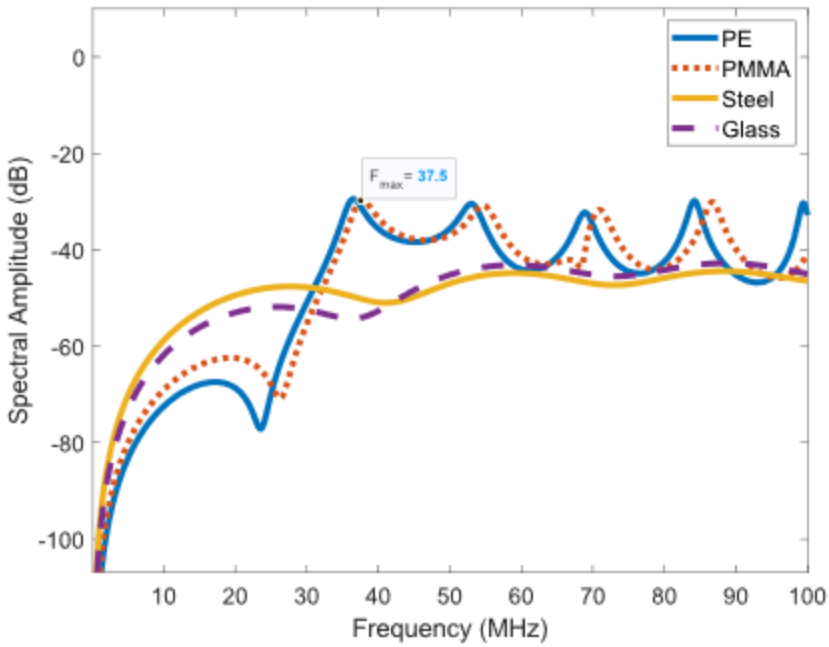

Figure 4

Scattering spectra of microspheres composed of different materials, computed over the 0–100 MHz range using Faran's theory. The model predicts the first resonance peak for PMMA microspheres at 37.5 MHz, establishing this frequency as the minimum threshold for reliable detection. Spectral analysis indicates that lower frequencies produce insufficient scattering, limiting their effectiveness for detecting 20 µm particles.

Supplementary Files

This is a list of supplementary files associated with this preprint. Click to download.

- SupplementaryInformation.docx